Food Chemistry 511 (2026) 148793

Contents lists available at ScienceDirect

Food Chemistry

journal homepage: www.elsevier.com/locate/foodchem

Mechanism and optimization of NaCl removal from soy sauce residue using low pressure superheated steam drying: Role of condensation and moisture migration

Xin Xu [a,1], Jian-Bo Liu [b,*,2], Jia-Cheng Guo [b], Zhi-Hong Xing [a], Rui-Fang Wang [a], Qing Xu [a,*,3]

[a] Tianjin Key Laboratory of Integrated Design and On-Line Monitoring for Light Industry and Food Machinery and Equipment, College of Mechanical Engineering, Tianjin University of Science and Technology, Tianjin 300222, China
[b] College of Engineering and Technology, Tianjin Agricultural University, Tianjin 300392, China

ARTICLE INFO

Keywords:
Soy sauce residue
Low-pressure superheated steam drying
NaCl migration
Moisture migration
Desalination

ABSTRACT

Soy sauce residue (SSR), a high-salt byproduct of condiment production, poses environmental and valorization challenges due to its NaCl content. The high salinity hinders its direct utilization in applications such as animal feed or fertilizer. This study introduces low-pressure superheated steam drying (LPSSD) for simultaneous dehydration and desalination. NaCl removal was driven by condensation-induced dissolution and steam-flow convection, with moisture as the key carrier. LPSSD achieved a 34.8% NaCl reduction, significantly surpassing vacuum drying ($p < 0.001$). Condensation and multi-stage condensation further enhanced desalination by rebuilding concentration gradients, while increased steam-material contact area improved efficiency. A robust kinetic model linked NaCl content to moisture ratio ($R^2 > 0.92$), revealing a three-stage process. Stratified experiments confirmed upward salt migration during condensation and convective transport thereafter. Compared with washing-based desalination, LPSSD can reduce wastewater generation associated with process water use and may provide an eco-friendlier alternative for SSR valorization.

1. Introduction

Amid escalating global warming and tightening natural resource constraints, improving the valorization of food-processing residues is increasingly important (Aschemann-Witzel, 2016). Soy sauce residue (SSR) is a major byproduct generated during soy sauce production across East and Southeast Asia(Gao et al., 2019). As illustrated in Fig. 1a, approximately 0.67 kg of SSR is generated per kilogram of soy sauce produced. China's annual soy sauce output has increased steadily in recent years, reaching 9 billion kilograms in 2023. Global annual soy sauce consumption is estimated at 10 billion liters (Zhou et al., 2021). SSR typically contains substantial salt and moisture, and residues from the high-salt liquid-state fermentation process (HSSF) exhibit particularly high moisture and salinity(Wang et al., 2021).

As depicted in Fig. 1b, SSR contains considerable crude protein, fat, fiber, and ash (21.8%, 29.2%, 18.1%, and 29.5% on a dry-weight basis) (Liu et al., 2017), indicating clear valorization potential, yet it is still largely discarded. High salinity constrains multiple utilization routes: as a fertilizer feedstock it may cause soil salinization(Shokri et al., 2024). In animal feed, excessive sodium intake can impair animal health (Faraco, 2024), and in anaerobic digestion, salinity inhibits microbial activity and reduces methane yield (Li et al., 2024). Concurrently, the high moisture content of SSR impedes transportation and storage(Xu, Liu, Xu, & Wang, 2025). Current industrial desalination approaches (Fig. 1c), mainly water washing and enzymatic hydrolysis, either consume large volumes of water and generate saline wastewater or incur high costs. Therefore, simultaneous reduction of salt and moisture is a prerequisite for improving SSR utilization.

Conventional drying techniques (e.g., hot air, vacuum drying) effectively remove moisture but exhibit negligible desalination efficacy. Preliminary research has indicated that low-pressure superheated steam (LPSSD) shows promise for the migration of both salts (Liu et al., 2017)

* Corresponding authors.
E-mail addresses: qingzhoujianbo@126.com (J.-B. Liu), xuqing@tust.edu.cn (Q. Xu).
[1] ORCID: https://orcid.org/0009-0008-6428-9495.
[2] ORCID: https://orcid.org/0000-0002-4084-4633.
[3] ORCID: https://orcid.org/0000-0001-9447-8117.

https://doi.org/10.1016/j.foodchem.2026.148793
Received 18 August 2025; Received in revised form 3 March 2026; Accepted 6 March 2026
Available online 10 March 2026
0308-8146/© 2026 Elsevier Ltd. All rights are reserved, including those for text and data mining, AI training, and similar technologies.

and sugars(Liu et al., 2024) in soy sauce residue; however, the detailed mechanisms underlying these processes remain unclear. Fig. 1d illustrates distinct drying stages and material temperature profiles under LPSSD conditions (Kittiworrawatt & Devahastin, 2009). As a drying medium for biomaterials, superheated steam offers additional advantages: superior product quality (Sehrawat et al., 2018), reduced oxidative degradation (Kheto et al., 2025), fire and explosion prevention, and significantly lower energy consumption (Linke & Kohlus, 2025). Liu et al. demonstrated effective sugar reduction in mango via LPSSD underscoring its process-specific adaptability for food applications (Liu et al., 2024).

However, mechanistic insights into salt migration within food waste remain scarce (Wang et al., 2019), particularly regarding NaCl migration during LPSSD. To narrow this gap, we investigated NaCl migration during LPSSD using two representative matrices: a liquid system (NaCl solution) to isolate interfacial dissolution/transport behavior, and a solid system (soy sauce residue, SSR) to capture salt redistribution within a porous food matrix. By analyzing mass balance, moisture evolution, NaCl removal, and stratified salt distributions under different condensation regimes and contact-area conditions, we propose a plausible mechanism for NaCl migration that is consistent with the observed experimental trends. These findings provide practical insights that could support the development of washing-free strategies for concurrent dehydration and desalination of soy sauce residue. The successful implementation of such a water-free process directly contributes to sustainable resource management by drastically reducing freshwater consumption and eliminating the generation of concentrated saline wastewater, thereby aligning with global efforts toward cleaner production and the valorization of waste streams within a circular economy.

2. Materials and methods

2.1. Materials

Fresh low-salt solid-state fermentation soy sauce residue (SSR) was supplied by Tianjin LiMin Condiment Co., Ltd. (Tianjin, China). Sodium chloride (NaCl, AR grade, ≥ 99.5% purity) and all other analytical grade chemicals were purchased from Fuchen Chemical Reagent Co., Ltd. (Tianjin, China). The silver nitrate standard solution (0.1 mol/L) used for chloride titration was also obtained from the same supplier. Third-grade laboratory deionized water was used for all solution preparation and extraction procedures throughout the study.

2.2. Methods

2.2.1. Preparation of SSR granules and NaCl solutions

Prior to experiments, low-salt solid-state SSR samples were pulverized using an FW100 mill (Tianjin Test Co., Ltd., China). The resulting powder was sieved through standard test sieves to isolate granules with particle sizes of 2-2.5 mm. Granules were sealed and stored in a freezer at 4 °C until use. Before processing, samples were thawed at 4 °C for 12 h to reach 25 °C, with an initial moisture content of 40 ± 3% (w.b.) (AOAC, 2023).

For liquid matrices, aqueous NaCl solutions were prepared by dissolving 0.01, 0.1, 1, or 5 g of NaCl (AR grade, ≥ 99.5% purity) separately in third-grade laboratory water, each made up to 100 mL to obtain final concentrations of 0.1, 1, 10, and 50 g/L, respectively.

2.2.2. Experimental system

The low-pressure superheated steam drying (LPSSD) apparatus used in this study was custom-engineered. A schematic is shown in Fig. 2 (see Fig. S1 for details). The system included a steam generator, a steam superheater, a vacuum drying chamber, a condensation system, a vacuum pump (BUCHI V-710, Switzerland), and an online data acquisition system (G&G, China). The steam generator supplied saturated steam at the system pressure. Steam temperature was controlled by an electric superheater with PID regulation to adjust the superheat level. The vacuum drying chamber had an internal volume of 300 mm × 300 mm × 275 mm. An electric heater was installed between its inner and outer shells. A perforated steam distributor (hole diameter 2 mm) was positioned above the sample stage. The sample stage was constructed from perforated polytetrafluoroethylene (PTFE) to maximize steam-sample contact. A material tray on this stage was connected to a real-time mass detector (G&G, China). Sample temperature was monitored using a K-type thermocouple inserted into the geometric center of a representative granule. Thermal insulation was applied to both the inner and outer surfaces of the drying chamber to minimize heat loss.

2.2.3. Drying methods

Soy sauce residue and saline solutions were treated using four methods: vacuum drying (VD), single-condensation LPSSD (LPSSD-C), non-condensable LPSSD (LPSSD-NC), and multi-condensation LPSSD (LPSSD-MC). To reach equilibrium temperature, the entire low-pressure

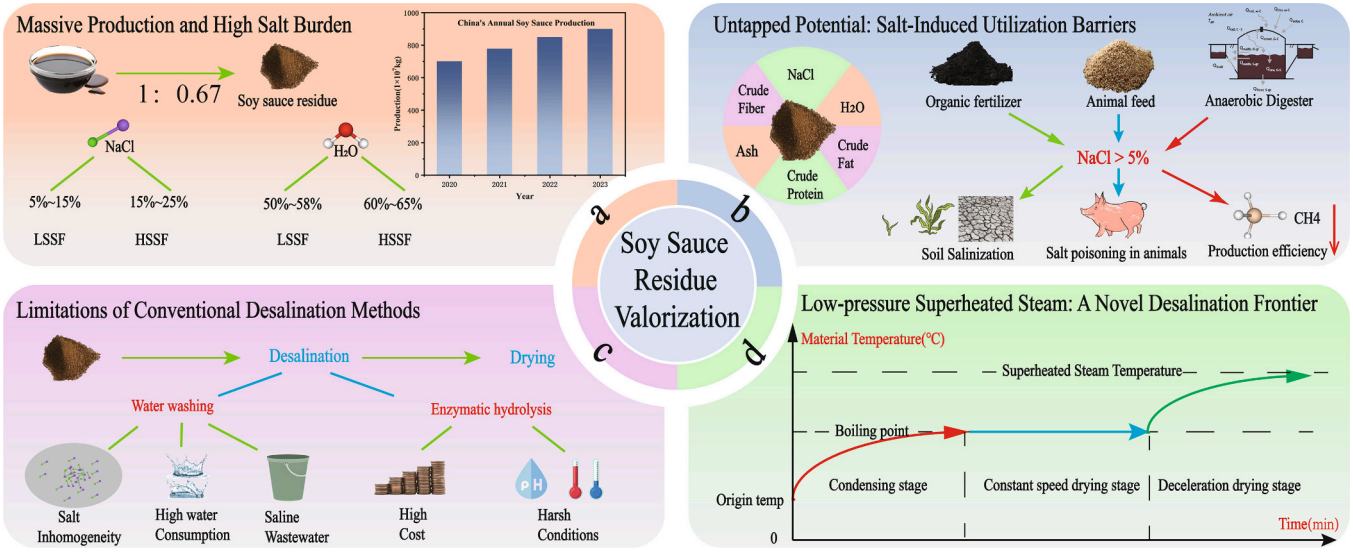


Fig. 1. Soy sauce residue valorization. (a). Massive production and high salt burden. (b). Untapped potential: Salt-induced utilization barriers. (c). Limitations of conventional desalination methods. (d). Low-pressure superheated steam: a novel desalination frontier.

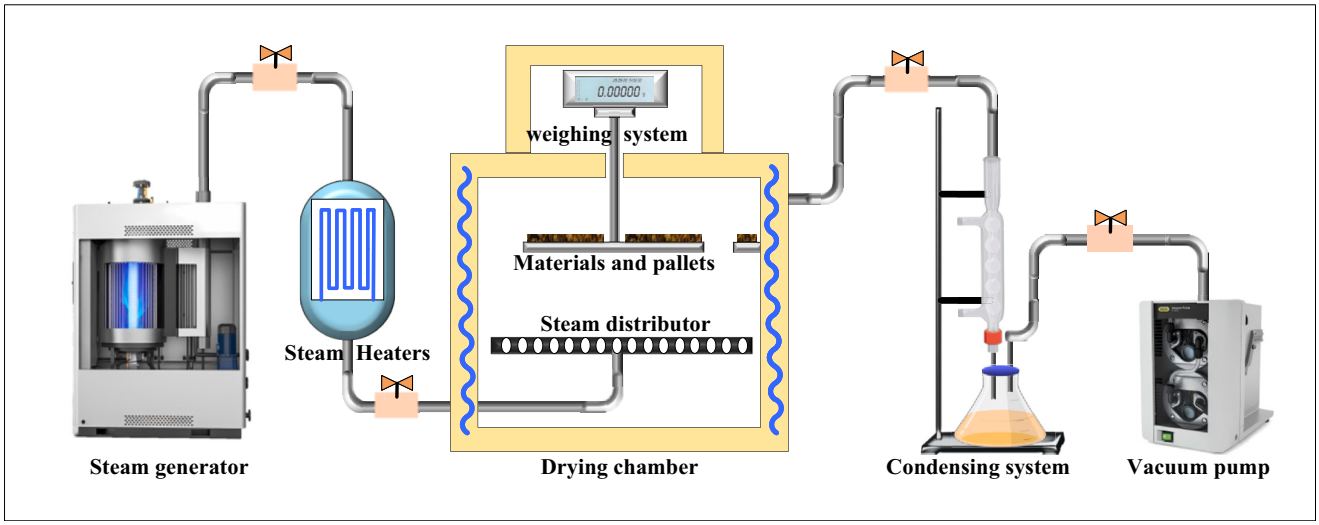


Fig. 2. Schematic diagram of the experimental setup.

superheated steam drying system was preheated for 30 min.

Previous studies have found that low-pressure superheated steam drying has elimination effects on sugars (Liu et al., 2024) and salts (Liu et al., 2017) but the deeper migration mechanism is not clear.

Therefore, this study aims to: (1) Study the mechanism of VD and low-pressure superheated steam drying on salt elimination in soy sauce residue; (2) Investigate the effect of the condensation process in low-pressure superheated steam drying on salt elimination in soy sauce residue; (3) Deepen the mechanism of salt migration in low-pressure superheated steam drying through the desalination and dehydration mechanism of liquid material (saline solution); (4) Establish a salt migration model for soy sauce residue in low-pressure superheated steam.

2.2.3.1. Vacuum drying (VD). To ensure comparability, vacuum drying (VD) was conducted in the same LPSSD system at 9 kPa, using identical chamber geometry, heating, and temperature monitoring. Steam injection was disabled to isolate the effect of the steam-flow environment. This approach eliminated systematic bias arising from equipment heterogeneity, such as differences in (VD) efficiency or sensor calibration (Skoog et al., 2017).

2.2.3.2. Single-condensation LPSSD (LPSSD-C). Single-condensation low-pressure superheated steam drying (LPSSD-C) represents the conventional LPSSD process. To ensure precise differentiation from non-condensable LPSSD (LPSSD-NC) and multi-condensation LPSSD (LPSSD-MC), it is designated as LPSSD-C.

SSR and saline solutions of varying concentrations were subjected to LPSSD-C treatment. The entire system was preheated to the target temperature and stabilized for 30 min. The vacuum pump was then activated to maintain a chamber pressure of 9 kPa. Prepared SSR samples (15 g) were placed on material trays positioned on the sample stage. Superheated steam was introduced at a flow rate of 3.5 g/min, and LPSSD-C continued until drying completion. The low steam flow rate and high-precision vacuum pump control preserved vacuum stability within the drying chamber (Liu et al., 2024).

2.2.3.3. Multi-condensation LPSSD (LPSSD-MC). To investigate the impact of condensation frequency on NaCl migration in SSR, multi-stage LPSSD (LPSSD-MC) was designed. Preliminary experiments revealed that material mass peaked at 2 min after steam injection and reverted to initial values at 10 min. This phenomenon stems from transient liquid film formation via steam condensation on cold SSR surfaces (causing mass increase), followed by film vaporization as material temperature reached the boiling point at chamber pressure (~43.8 °C at 9 kPa). Mass recovery marked condensation termination, yet residual films persisted (Xu, Liu, Zhang, et al., 2025), due to higher internal moisture migration rates versus surface evaporation (Pai et al., 2021). Thus, a single condensation cycle duration was fixed at 10 min for 15 g SSR at 25 °C.

Operational sequence (identical preheating/startup to LPSSD-C): (1) At 10 min: Samples removed (timing paused) and cooled to 25 °C. (2) LPSSD treatment reinitiated. (3) At 20 min (i.e., after 10-min interval): Samples retrieved for NaCl content and moisture ratio analysis (second condensation cycle). Steps 1–3 repeated with 10-min cycle intervals until wet-basis moisture content plateaued.

2.2.3.4. Non-condensable LPSSD drying (LPSSD-NC). To establish a "non-condensable" condition and prevent significant steam condensation on the sample, the following procedure was used. The entire system was preheated to 90 °C for 30 min. Prepared SSR (15 g) was loaded onto material trays and positioned on the sample stage (see S2.3). The vacuum pump was activated to reduce system pressure to 9 kPa, followed by 5-min vacuum preheating of samples. At this stage, SSR temperature exceeded the boiling point at system pressure (~43.8 °C). Superheated steam was then introduced at 3.5 g/min, with continuous mass recording until drying completion.

This procedure prevented significant liquid accumulation because preheated samples surpassed the pressure-dependent boiling point. Microscopically, while steam condensation occurred on surfaces, concurrent vaporization of surface water maintained a dynamic equilibrium.

2.2.4. Moisture content determination

2.2.4.1. Moisture content (MC, wet basis). The moisture content was determined by drying 5 g samples in a hot-air oven at 105 °C. Samples were weighed every 30 min after the initial 2-h drying period until constant mass was achieved. The initial wet-basis moisture content of soy sauce residue was measured as 40 ± 3% prior to experiments. The moisture content (wet basis) is calculated as follows (AOAC, 2023; Getahun & Ebissa, 2024):

$$M_t = \frac{m_t - m_d}{m_t} \times 100\% \quad (1)$$

where: M_t is moisture content (wet basis) at time t, g•g^{-1}(w.b.); m_t is sample mass at time t, g; m_d oven-dry mass of sample, g.

2.2.4.2. Moisture ratio(MR). The moisture ratio (MR) of SSR was

calculated according to Eq. (2) (Thorat et al., 2012; Zang et al., 2023):

$$MR = \frac{X_t - X_e}{X_0 - X_e} \quad (2)$$

where, X_t is the moisture content at time t, $g{\cdot}g^{-1}$(d.b.); X_e is the equilibrium moisture content of the material, $g{\cdot}g^{-1}$(d.b.); X_0 is the initial dry basis moisture content of the material, $g{\cdot}g^{-1}$(d.b.).

2.2.5. NaCl content and removal efficiency

2.2.5.1. NaCl content in solution. The argentometric titration method is widely recognized for measuring Cl^- content in liquids (Kolb et al., 2017). NaCl solutions after experimental treatment were analyzed by silver nitrate titration. Triplicate measurements were performed for each group, with arithmetic mean values adopted. The NaCl content is expressed by Eq. (3):

$$C_{NaCl} = \frac{(V_2 - V_1) \times M \times 35.45 \times 1000}{V} \quad (3)$$

where, V_1 is the volume of silver nitrate standard solution consumed by distilled water, mL; V_2 is the volume of silver nitrate standard solution consumed by the sample, mL; M is the concentration of silver nitrate standard solution, mol/L; V is the volume of the sample, mL.

2.2.5.2. NaCl content in soy sauce residue. The sodium chloride content in soy sauce residue was determined by chloride ion quantification using a calibrated chloride ion-selective electrode (ISE) (Zhao et al., 2024). Briefly, continuous aqueous extraction was performed on dried samples. Each extraction step consisted of 15-min ultrasonication in 200 mL (first step) or 100 mL (subsequent steps) of deionized water, followed by vacuum filtration. The filtrate volume was precisely measured, and chloride ion concentration was immediately determined by ISE. The mass of chloride ions recovered in each filtrate was calculated as the product of concentration and filtrate volume.

This extraction process was iteratively conducted: the residue from the first filtration underwent a second extraction with 100 mL deionized water, and the residue from the second extraction was subjected to a third extraction. Analysis of the fourth extract confirmed that chloride ion concentration was indistinguishable from that of the deionized water blank; therefore, three extraction cycles were employed to ensure complete extraction while minimizing procedural steps. The total chloride mass recovered from the first three successive extracts equated to the chloride content of the original sample and was converted to equivalent sodium chloride mass. (See S2.2 for more detailed operation procedures).

$$m_{NaCl,n} = C_n \times V_n \times 58.45 \quad (4)$$

$$m_{NaCl} = \sum_{n=1}^{3} m_{NaCl,n} \quad (5)$$

where, m_{NaCl} is the NaCl content in the material, g; $m_{NaCl,n}$ is the NaCl content in the n-th filtrate, g; C_n is the Cl^- concentration in the n-th filtrate, mol/L; V_n is the volume of the n-th filtrate, L.

2.2.5.3. NaCl removal rate. The NaCl removal rate was calculated using Eq. (6):

$$R = \frac{m_{NaCl,initial} - m_{NaCl,final}}{m_{NaCl,initial}} \times 100\% \quad (6)$$

where, $m_{NaCl,final}$ is the NaCl content in the material after treatment, g; $m_{NaCl,initial}$is the initial NaCl content in the material, g.

2.2.6. Data analysis

The experimental data, expressed as the mean of three determinations ± standard deviation, were analyzed by one-way ANOVA. When significant differences were found ($p < 0.05$), Duncan's multiple range test was applied for post-hoc comparisons using SPSS statistics software (Version 21.0, SPSS Inc., Chicago, IL, USA).

3. Results and discussion

3.1. Desalination behavior of SSR under LPSSD

3.1.1. NaCl removal behavior under LPSSD

Fig. 3 illustrates the influence of drying environment, steam-material contact, and condensation history on NaCl removal from SSR. In VD, NaCl content did not significantly decrease ($p > 0.05$) despite rapid moisture loss (Fig. 3a and Fig. S2). This indicates that moisture and salt transport are decoupled under VD. Under VD, moisture removal from SSR is driven by vapor-pressure-driven phase change (Eq. S1) (Cáceres et al., 2007; Chahbani et al., 2018). In contrast, NaCl migration is diffusion-limited, following the much slower Fick-type transport (Eq. S2) (Gerla & Rubiolo, 2003). This mechanistic divergence explains why VD achieves dehydration but not significant desalination.

LPSSD achieved significantly greater NaCl removal than VD. The dry-basis NaCl content decreased to 16.17 ± 0.17% under LPSSD-NC and to 15.01 ± 0.15% under LPSSD-C (Fig. 3a). This result establishes a clear efficacy order: LPSSD-C > LPSSD-NC > VD. This hierarchy reveals two underlying mechanisms. First, the flowing superheated steam provides interfacial shear (drag). This shear force convectively displaces surface solutes through forced-convection mass transfer (Eq. S3) (Poós & Varju, 2024), an effect absent in VD. Second, in LPSSD-C, steam condensation on the cold SSR forms a transient liquid film (Kittiworrawatt & Devahastin, 2009). This film dissolves NaCl (Eq. S2) and renews the surface concentration gradient, thereby enhancing diffusion and promoting subsequent convective salt removal.

Contact-area experiments provided direct evidence for the interfacial control of NaCl removal under LPSSD. Increasing the steam-material contact area consistently reduced residual NaCl content in LPSSD, while VD showed only marginal improvement (Fig. 3b). This result aligns with the established dependence of convective mass-transfer coefficients on interfacial scale and flow conditions (Eq. S3) (Karabulut & Alnak, 2024).

LPSSD-MC further decreased the dry-basis NaCl content to 13.82 ± 0.12% (Fig. 3c, d). Most desalination occurred during the initial cycles. The periodic regeneration of surface condensate films in this process reconstructs concentration gradients. This sustains non-steady-state diffusion (Eq. S2) and promotes salt migration from deeper regions (Zhang et al., 2024).

3.1.2. Effect of initial moisture content on NaCl removal

The initial moisture content (M_0) significantly influenced final dry-basis NaCl levels (Fig. 3h). When M_0 increased from 40% to 50.5%, the final NaCl content decreased from 15.01% to 14.32% ($p < 0.05$). However, continued steam exposure after drying did not further reduce NaCl (Fig. 3g).

These results confirm that water acts as an essential carrier for NaCl migration. A higher M_0 increases the free water content within SSR, which establishes continuous aqueous pathways. These pathways enable the convective co-transport of dissolved NaCl toward the material surface. Consequently, once the internal moisture migration ceases, the forced convective removal of NaCl also stops abruptly.

3.2. Desalination analysis of saline solutions

3.2.1. Vacuum heating and LPSSD treatment analysis

NaCl solution desalination was systematically compared under VD and LPSSD to isolate the role of the gaseous-phase kinetic environment (Fig. 4). VD treatment resulted in only marginal NaCl reduction over time ($p > 0.05$). In contrast, LPSSD induced significant, concentration-

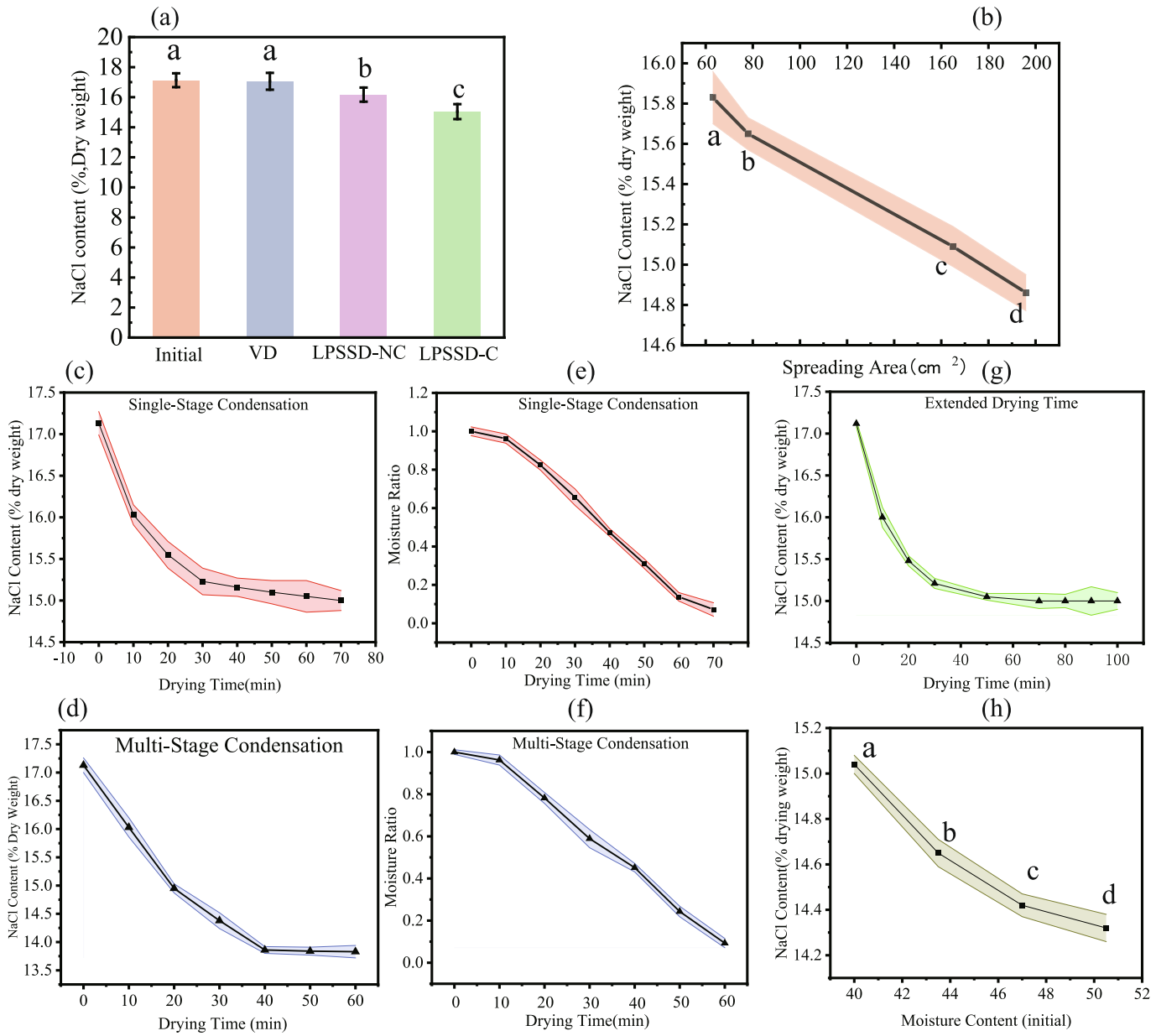


Fig. 3. (a). Effects of different drying methods on NaCl content in SSR. (b). Effect of spreading area on NaCl content in SSR. (c). Salt content variation over time during LPSSD-C. (d). Salt content variation over time during LPSSD-MC. (e). Moisture ratio variation over time during LPSSD-C. (f). Moisture ratio variation over time during LPSSD-MC. (g). Effect of extended drying time on salt content. (h). Relationship between initial moisture content and final NaCl content.

dependent declines. At a steam flow of 1.5 g/min (generator temperature 80 °C), NaCl removal increased with solution concentration (Fig. 4a). A higher steam flow of 3.5 g/min (90 °C) further enhanced the removal across all concentrations (Fig. 4b). Specifically, increasing the flow from 1.5 to 3.5 g/min raised the NaCl removal rate after 2 h by 2.52% to 5.12% across the tested range (0.1–50 g/L). However, this enhancement did not scale linearly with the flow increase, indicating diminishing returns and a tendency toward a transport-limited regime at higher flows. The improved removal is attributable to greater interfacial shear (drag force) and volumetric steam displacement under the higher flow condition.

The solution-phase results align with the SSR drying observations. Both systems demonstrate that VD cannot achieve concurrent dewatering and desalination, as it relies solely on slow diffusion. LPSSD, however, enables efficient co-removal through the mechanical action of flowing steam, which exerts shear and drag forces to displace dissolved NaCl from the material interface.

3.2.2. *Interfacial area enhancement mechanism for NaCl migration*

To investigate how interfacial area regulates NaCl migration, 0.2 g/L NaCl solutions were treated in circular vessels of different diameters under LPSSD or VD. A 36% increase in the interfacial area raised the NaCl removal rate from 18.3% to 34.7% under LPSSD ($p < 0.001$) (Fig. 5). In contrast, VD showed negligible improvement (< 2%).

This result is consistent with observations from SSR drying. For VD, the limited enhancement is attributed to a shortened diffusion path length. For LPSSD, the marked improvement stems from the intensified mechanical action (shear/drag forces) of flowing steam at the expanded interface. This contrast further confirms that VD is ineffective for concurrent dewatering and desalination, whereas LPSSD effectively couples both processes.

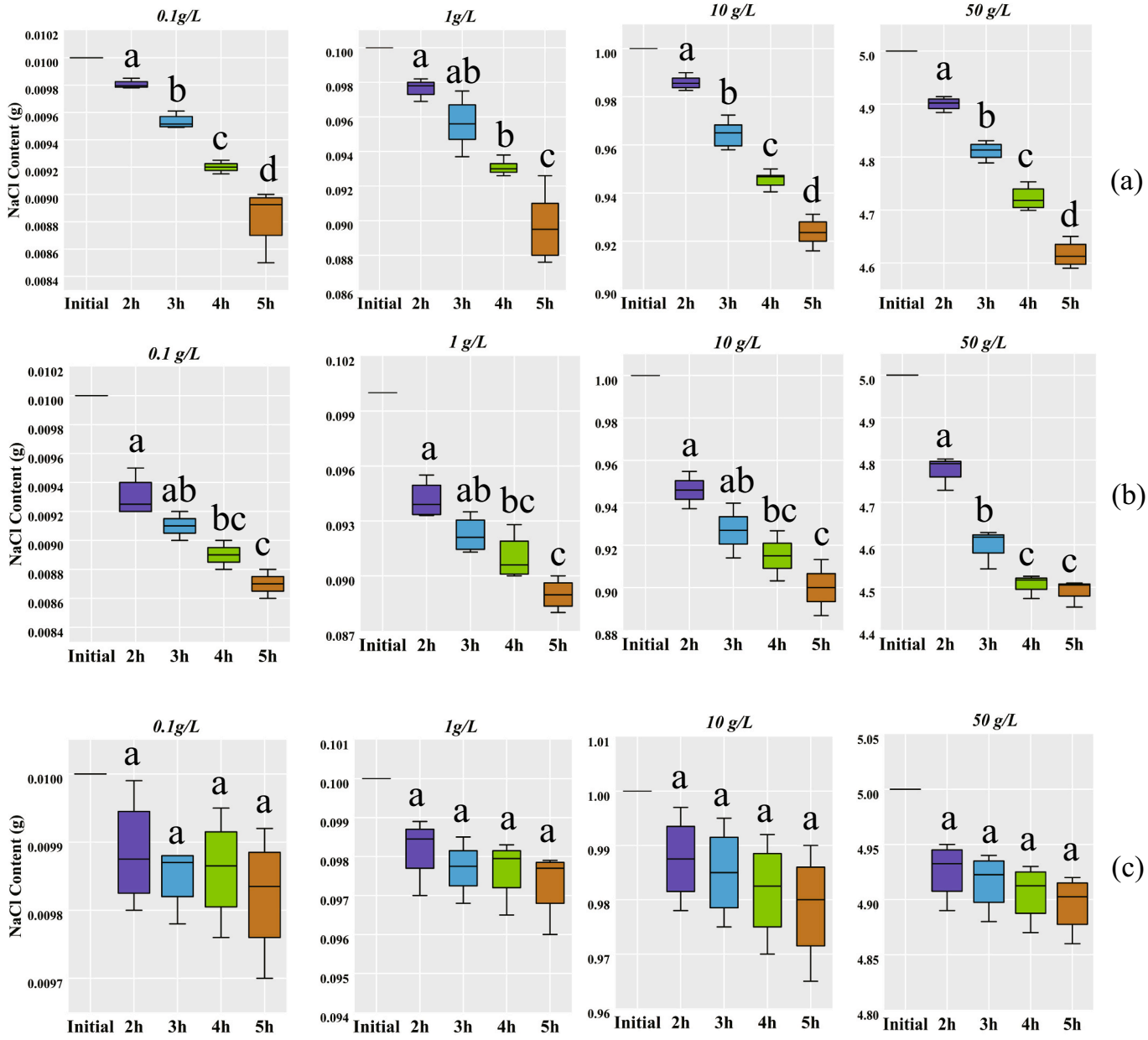


Fig. 4. Temporal variation of NaCl content in solutions under different drying conditions. (a) LPSSD with a steam flow of 1.5 g/min. (b) LPSSD with a steam flow of 3.5 g/min. (c) VD (control, no steam flow).

3.3. NaCl migration patterns in SSR under LPSSD

3.3.1. Kinetic stage model of NaCl migration

A strong coupling was observed between NaCl migration and moisture ratio (MR) under LPSSD, with the kinetic profile further modulated by condensation conditions (Fig. 6c and Fig. 6e). The relationship under LPSSD-NC was modeled as a monotonic function (Eq. 7), while the data under LPSSD-C required a three-segment model (Eq. 8) describing rapid, steady, and slow desalination stages. The fitted parameters for both models are summarized in Table S1.

$$y = 1.26x^2 - 0.2304x + 16.14 \tag{7}$$

where x is the moisture ratio, dimensionless; y is the NaCl content.

$$y = \begin{cases} 96.2x^2 - 182.4x + 102.5, & x > 0.96 \quad \text{(Rapid)} \\ 4.844x^2 - 5.136x + 16.5, & 0.65 < x \le 0.96 \quad \text{(Stationary)} \\ 0.2987x^2 - 0.1594x + 14.99, & x \le 0.65 \quad \text{(Slow)} \end{cases} \tag{8}$$

where, x denotes the moisture ratio and y denotes the NaCl content.

Both regression models showed high predictive capability, with coefficients of determination (R^2) exceeding 0.92 (Table S1). This performance was further validated by comparing model predictions against experimentally measured NaCl contents at key drying time points (Table 1). For both the LPSSD-NC and LPSSD-C models, the maximum absolute error was ≤1.7%, confirming their satisfactory accuracy for practical use.

The established quantitative relationship between MR and NaCl content provides a predictive tool for salt migration dynamics. It offers a valuable kinetic framework for analyzing the transport of water-soluble components in porous materials during superheated steam processing.

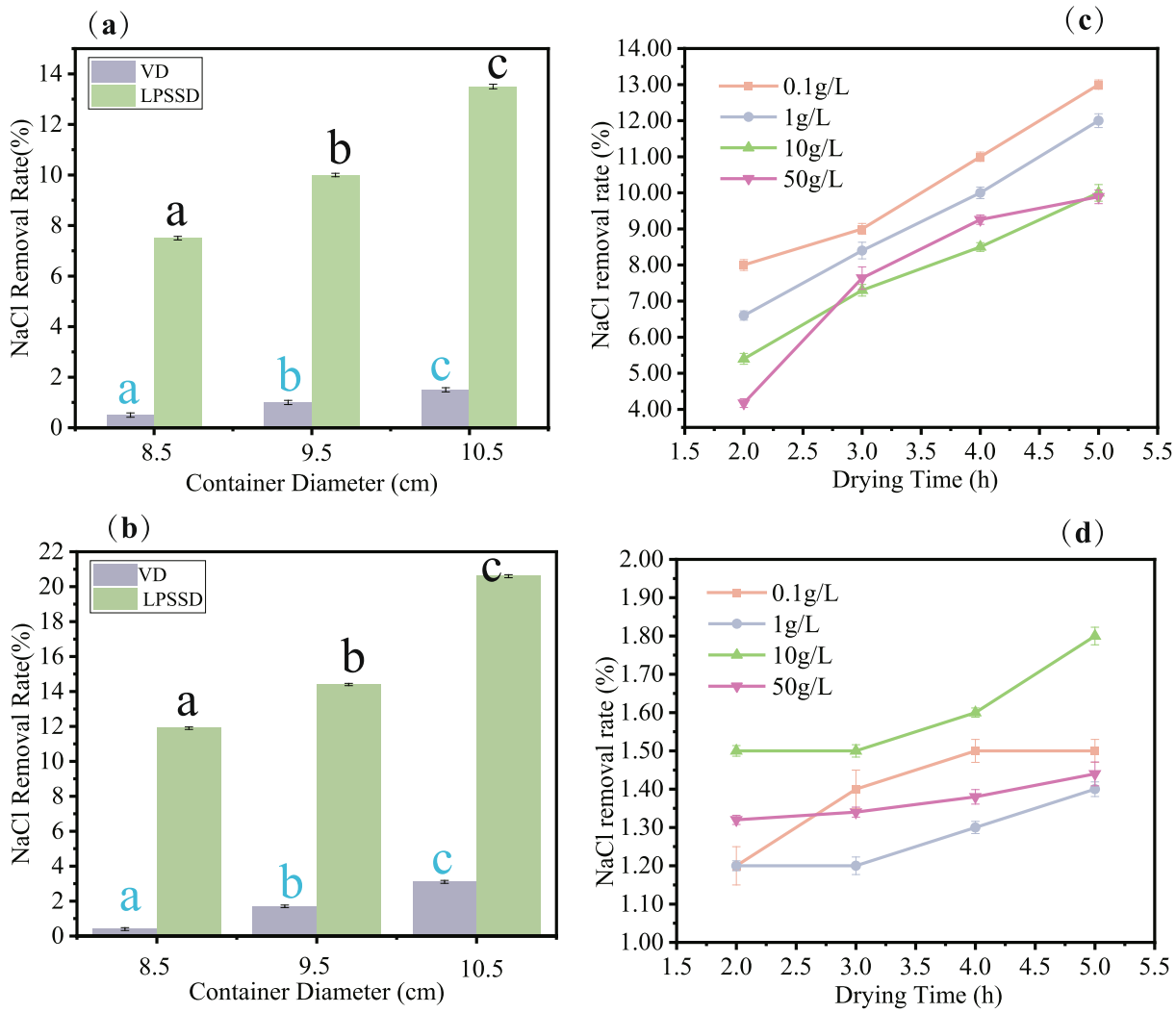


Fig. 5. (a). Effect of spreading area on NaCl removal rate from salt solution (0.2 g/L). (b). Effect of spreading area on NaCl removal rate from salt solution (1 g/L). (c). NaCl removal rate variation over time during LPSSD at 90 °C for brine solutions of different concentrations. (d). NaCl removal rate variation over time during VD at 90 °C for brine solutions of different concentrations.

3.3.2. Stratified migration mechanism and condensation–convection synergistic effect

To elucidate the spatial dynamics of NaCl migration, SSR was stratified into upper and lower layers and treated under LPSSD-C. The temporal evolution of moisture content (MC) and NaCl content in each layer was tracked (Fig. 6a, d, e), with the initial 6-min changes detailed in Fig. 6f. This analysis revealed distinct, stage-dependent transport mechanisms. Analysis of the stratified data (Table 2, Table S2) identified four sequential stages:

(1) Condensation-dominated stage (0–2 min): Steam condensation formed a liquid film on the upper layer. The resulting low chemical potential drove the upward dissolution and migration of NaCl from the lower layer.

(2) Convective shear-dominated stage (2–5 min): As the surface film evaporated, the moisture content remained higher in the upper layer. The primary driver for NaCl migration shifted to the mechanical shear (drag) exerted by the flowing steam.

(3) Concentration-driven redistribution stage (10–15 min): After significant desalination of the upper layer, a transient concentration trough formed. This established a new chemical potential gradient, triggering compensatory diffusion of NaCl from the lower layer until a local equilibrium was approached.

(4) Coupled decline stage (to completion): Thereafter, under the sustained action of flowing steam, both moisture and NaCl in both layers decreased gradually until drying ended.

This stage-resolved analysis, summarized in Fig. 7, demonstrates the synergistic and time-varying roles of condensation and convection. The process hinges on the initial condensate film creating a pathway for dissolution, followed by steam-driven shear and re-established diffusion gradients to promote continuous salt displacement. These insights provide a mechanistic foundation for the simultaneous dehydration and desalination of SSR and similar high-salt matrices via LPSSD.

3.4. Limitations and future work

The mechanistic interpretation in this study is primarily inferred from macroscopic observables (mass balance, bulk NaCl content, moisture ratio evolution, and stratified layer measurements) rather than from direct in situ characterization at the interface. Specifically, the surface liquid film thickness, local NaCl concentration gradients, and interfacial shear/velocity fields were not directly quantified in the current setup. Therefore, the proposed dissolution–carriage pathway should be regarded as a plausible mechanism consistent with the observed trends. Future work will integrate in situ film visualization and local concentration profiling, and may incorporate flow-field quantification and CFD-assisted analysis to further validate and parameterize the

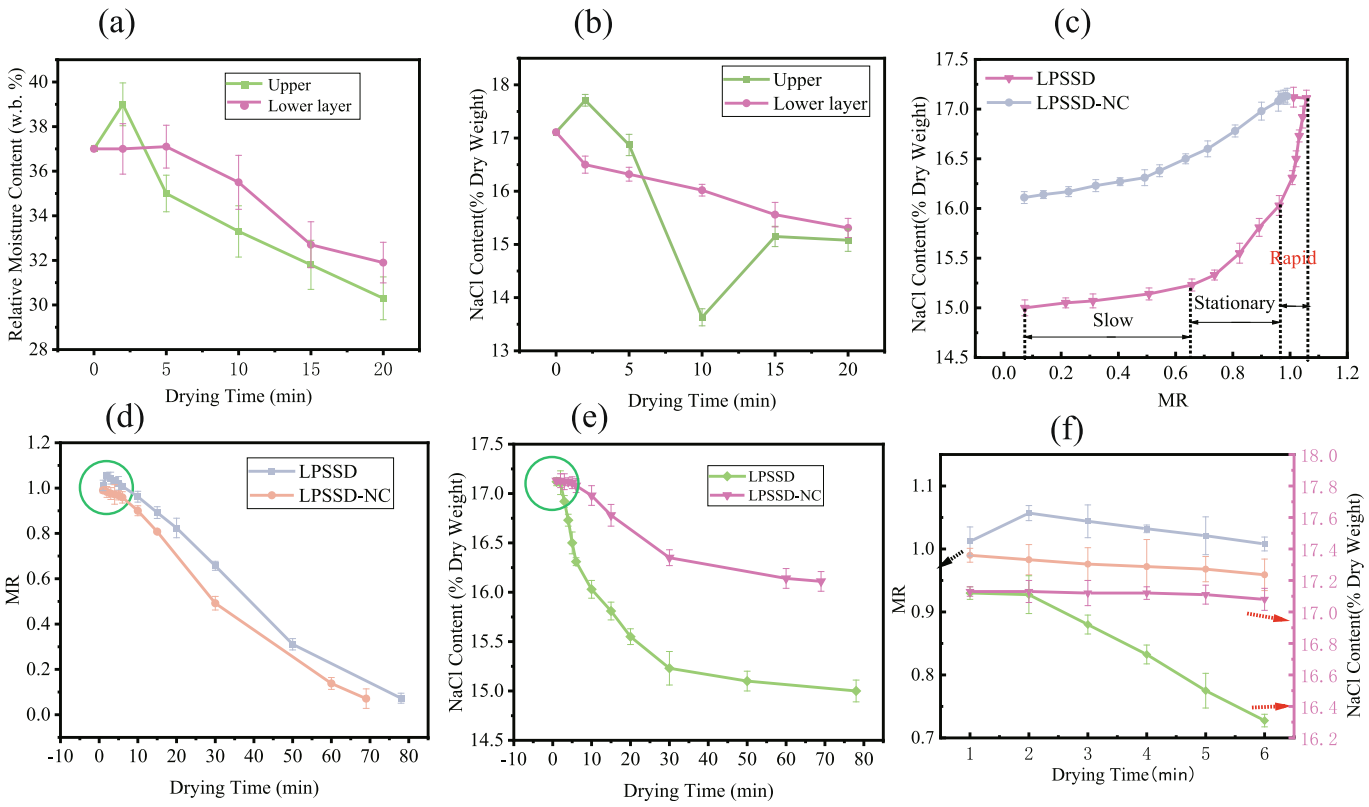


Fig. 6. Dynamics of moisture and NaCl migration in stratified SSR during LPSSD. (a) Temporal evolution of moisture ratio (MR) in the upper and lower layers. (b) Temporal evolution of NaCl content in the upper and lower layers. (c) Fitted relationship between NaCl content and moisture ratio under LPSSD-C and LPSSD-NC conditions. (d) Comparison of moisture ratio over drying time between LPSSD and LPSSD-NC. (e) Comparison of NaCl content over drying time between LPSSD and LPSSD-NC. (f) Enlarged view of the initial 6 min showing the temporal variation of moisture ratio and NaCl content for LPSSD and LPSSD-NC.

Table 1
Regression model validation.

Drying methods	MR	Actual NaCl content(%, db.)	Predicted NaCl content(%, db.)	Absolute error
	0.862	16.70	16.88	1.1%
LPSSD-NC	0.538	16.50	16.38	0.7%
	0.198	16.11	16.14	0.2%
	0.980	15.87	16.14	1.7%
LPSSD-C	0.752	15.26	15.38	0.5%
	0.210	15.00	14.97	0.2%

Table 2
Layer-specific phenomena and driving mechanisms in soy sauce residue during LPSSD-C.

Layer	Phenomena	Driving Mechanism
Upper Layer	0-2 min: Forms surface condensate film.	Condensation-Dissolution: Steam condensation creates liquid film dissolving NaCl.
	2–5 min: Film evaporation; retains higher moisture than lower layer.	Chemical potential gradient (Δμ): Low chemical potential in film drives upward NaCl migration.
	>10 min: Develops transient concentration trough post-desalination.	Forced convective shear: High-velocity steam removes solutes.
Lower Layer	0–2 min: NaCl migrates upward.	Concentration gradient diffusion: Δμ drives Fickian diffusion upward.
	2–10 min: Continuous upward NaCl migration under steam shear.	Forced convective transport: Steam shear overcomes diffusion resistance.
	>10 min: Compensatory diffusion toward concentration trough.	Compensatory diffusion: Δμ equilibration until chemical potential balance.

interfacial mass-transfer mechanism.

Energy largely tracks the evaporation load. LPSSD can lower net demand when condenser heat is recovered and steam utilities are integrated. Otherwise, energy should be considered similar to other low-pressure dryers. Multi-condensation (six cycles) served to illustrate gradient reconstruction; because gains diminish after early cycles, repeated cooling/restarting is impractical at scale and could be replaced by multi-zone operation (cold-feed condensation followed by superheated-steam drying).

To further investigate the fate of removed NaCl, condensate from LPSSD runs was analyzed. Under standard experimental conditions, NaCl concentration was below the detection limit, which is consistent with the expected deposition of salt-laden aerosols within the apparatus or potential volatilization. Only when processing SSR with artificially elevated salt concentrations were trace amounts of NaCl detectable in the condensate. This confirms that the primary fate of the convectively transported salt under typical conditions is not transfer into the condensate stream. Future industrial implementations of this concept would benefit from integrating a dedicated salt recovery or crystallization unit downstream.

3.5. *Novelty impact statement*

This work first clarifies the NaCl migration mechanism in soy sauce residue during low-pressure superheated steam drying (LPSSD). The key novelty lies in the synergistic condensation-convection effect that achieves concurrent dehydration and desalination without process water, thereby preventing saline wastewater generation. A predictive kinetic model is established. These findings advance the understanding of salt migration and offer a scalable, eco-friendly strategy for the valorization of high-salt food byproducts (see Supplementary Material S4 for

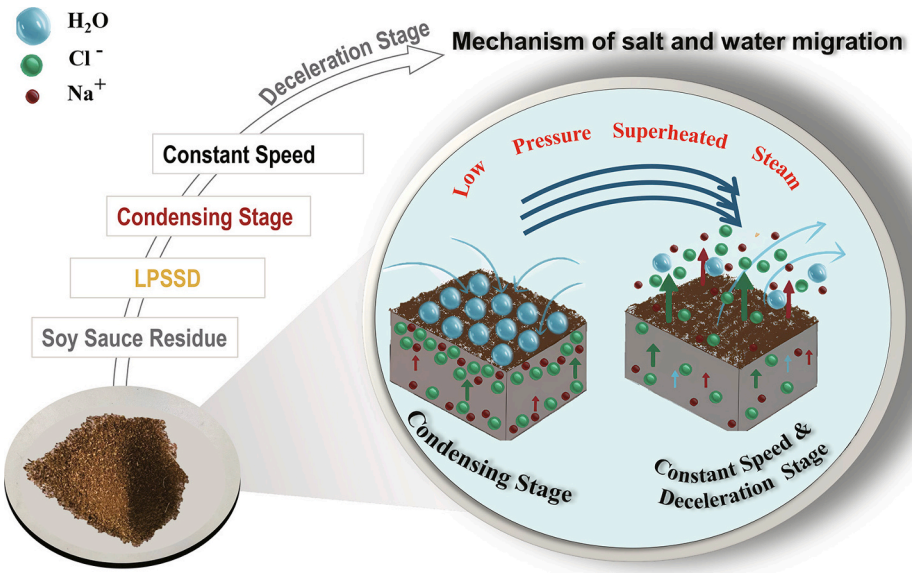


Fig. 7. Schematic diagram of salt and moisture migration mechanisms during low-pressure superheated steam drying (LPSSD) of soy sauce residue.

alignment with UN Sustainable Development Goals).

4. Conclusion

This study demonstrates that low-pressure superheated steam drying (LPSSD) effectively achieves simultaneous dehydration and desalination of soy sauce residue. LPSSD reduced the NaCl content in dried SSR by 34.8%, a significant improvement over vacuum drying which removed moisture but exhibited negligible desalination.

The success of LPSSD hinges on a synergistic mechanism: initial steam condensation dissolves surface salt, and subsequent steam flow provides the mechanical shear needed to displace it, with internal moisture migration acting as the essential carrier. This mechanistic understanding was further validated by the enhanced efficiency achieved through increased interfacial area and multi-stage condensation.

Beyond SSR, this LPSSD-based approach presents a scalable, eco-friendly alternative to water-intensive washing for high-salt food byproducts. By eliminating process water and preventing concentrated saline wastewater generation, it aligns with cleaner production goals and supports the sustainable valorization of industrial food residues within a circular economy framework.

CRediT authorship contribution statement

Xin Xu: Writing – original draft, Visualization, Software, Conceptualization. **Jian-Bo Liu:** Writing – original draft, Supervision, Funding acquisition, Conceptualization. **Jia-Cheng Guo:** Software, Formal analysis. **Zhi-Hong Xing:** Formal analysis, Data curation. **Rui-Fang Wang:** Supervision, Methodology. **Qing Xu:** Writing – review & editing, Supervision.

Declaration of competing interest

The authors declare that they have no known competing financial interests or personal relationships that could have appeared to influence the work reported in this paper.

Acknowledgments

The authors express their appreciation to the Development Fund Project for Young Scientific and Technological Talents of Tianjin Agricultural College (Grant No. 2025QNKJ13) and the Scientific Research Projects of Tianjin Municipal Education Commission (Contract No. 2023ZD002).

Appendix A. Supplementary data

Supplementary data to this article can be found online at https://doi.org/10.1016/j.foodchem.2026.148793.

Data availability

Data will be made available on request.

References

AOAC. (2023). *Official methods of analysis* (22nd Edition. In). Rockville, MD, USA: AOAC.
Aschemann-Witzel, J. (2016). Waste not, want not, emit less. *Science, 352*(6284), 408–409. https://doi.org/10.1126/science.aaf2978
Cáceres, G., Bruneau, D., & Jomaa, W. (2007). Two-phase shrinking porous media drying:: A modeling approach including liquid pressure gradients effects. *Drying Technology, 25*(12), 1927–1934. https://doi.org/10.1080/07373930701727226
Chahbani, A., Fakhfakh, N., Balti, M. A., Mabrouk, M., El-Hatmi, H., Zouari, N., & Kechaou, N. (2018). Microwave drying effects on drying kinetics, bioactive compounds and antioxidant activity of green peas (Pisum sativum L.). *Food Bioscience, 25*, 32–38. https://doi.org/10.1016/j.fbio.2018.07.004
Faraco, G. (2024). Dietary salt, vascular dysfunction, and cognitive impairment. *Cardiovascular Research, 120*(18), 2349–2359. https://doi.org/10.1093/cvr/cvae229
Gao, X., Zhang, J., Liu, E., Yang, M., Chen, S., Hu, F., … Yu, X. (2019). Enhancing the taste of raw soy sauce using low intensity ultrasound treatment during moromi fermentation [article]. *Food Chemistry, 298, Article 124928*. https://doi.org/10.1016/j.foodchem.2019.05.202
Gerla, P. E., & Rubiolo, A. C. (2003). A model for determination of multicomponent diffusion coefficients in foods. *Journal of Food Engineering, 56*(4), 401–410. article Pii s0260-8774(02)00213-3 https://doi.org/10.1016/s0260-8774(02)00213-3.
Getahun, E., & Ebissa, D. T. (2024). Investigation of optimal drying conditions of red chili peppers in a hot air cabinet dryer. *Case Studies in Thermal Engineering*. https://doi.org/10.1016/j.csite.2024.104586, 59, Article 104586.
Karabulut, K., & Alnak, Y. (2024). Investigation of forced convection heat and moisture transfer for semi-circular moist objects by using an impinging hot air jet flow. *International Journal of Heat and Fluid Flow, 109, Article 109526*. https://doi.org/10.1016/j.ijheatfluidflow.2024.109526
Kheto, A., Sehrawat, R., Gul, K., & Devahastin, S. (2025). Unveiling the impact of superheated steam treatment on nutritional, functional and rheological behavior of guar germ protein isolates [article]. *Food Hydrocolloids, 166, Article 111383*. https://doi.org/10.1016/j.foodhyd.2025.111383
Kittiworrawatt, S., & Devahastin, S. (2009). Improvement of a mathematical model for low-pressure superheated steam drying of a biomaterial. *Chemical Engineering Science, 64*(11), 2644–2650. https://doi.org/10.1016/j.ces.2009.02.036
Kolb, M., Bahadir, M., & Teichgräber, B. (2017). Determination of chemical oxygen demand (COD) using an alternative wet chemical method free of mercury and dichromate. *Water Research, 122*, 645–654. https://doi.org/10.1016/j.watres.2017.06.034

Li, Z. Y., Nagao, S., Inoue, D., & Ike, M. (2024). Different inhibition patterns of ammonia and salt revealed by kinetic analysis of their combined inhibitory effect on methanogenesis of hydrogen: A preliminary study. *Biochemical Engineering Journal, 205, Article 109263*. https://doi.org/10.1016/j.bej.2024.109263

Linke, T., & Kohlus, R. (2025). Pre-gelatinisation of native potato starch by thermal treatment in a pilot-scale superheated steam spray drying system [article]. *Innovative Food Science & Emerging Technologies, 102, Article 103993*. https://doi.org/10.1016/j.ifset.2025.103993

Liu, J., Xu, X., Zhang, T., Wang, J., Wang, R., & Xu, Q. (2024). Combined effects of low pressure superheated steam drying and vacuum drying on sugar reduction and quality attribute in mango (*Mangifera indica L.*) slices [Article]. *International Journal of Food Engineering, 20*(6), 405–417. https://doi.org/10.1515/ijfe-2023-0249

Liu, J., Zang, L., Xu, Q., Wang, R., & Li, Z. (2017). Drying of soy sauce residue in superheated steam at atmospheric pressure [article]. *Drying Technology, 35*(13), 1656–1663. https://doi.org/10.1080/07373937.2016.1273232

Pai, K. R., Sindhuja, V., Ramachandran, P. A., & Thorat, B. N. (2021). Mass transfer "regime" approach to drying. *Industrial & Engineering Chemistry Research, 60*(26), 9613–9623. https://doi.org/10.1021/acs.iecr.1c01680

Poós, T., & Varju, E. (2024). New dimensionless equation for mass transfer at acetone evaporation under forced convection. *International Communications in Heat and Mass Transfer, 159, Article 107961*. https://doi.org/10.1016/j.icheatmasstransfer.2024.107961

Sehrawat, R., Nema, P. K., & Kaur, B. P. (2018). Quality evaluation and drying characteristics of mango cubes dried using low-pressure superheated steam, vacuum and hot air drying methods. *LWT- Food Science and Technology, 92*, 548–555. https://doi.org/10.1016/j.lwt.2018.03.012

Shokri, N., Hassani, A., & Sahimi, M. (2024). Multi-scale soil salinization dynamics from global to pore scale: A review [review]. *Reviews of Geophysics, 62(4), Article e2023RG000804*. https://doi.org/10.1029/2023rg000804

Skoog, D. A., Holler, F. J., & Crouch, S. R. (2017). *Principles of instrumental analysis* (7th ed.). Cengage Learning.

Thorat, I. D., Mohapatra, D., Sutar, R. F., Kapdi, S. S., & Jagtap, D. D. (2012). Mathematical Modeling and experimental study on thin-layer vacuum drying of ginger (Zingiber Officinale R.) slices. *Food and Bioprocess Technology, 5*(4), 1379–1383. https://doi.org/10.1007/s11947-010-0429-y

Wang, X., Guo, M., Song, H., Meng, Q., & Guan, X. (2021). Characterization of key odor-active compounds in commercial high-salt liquid-state soy sauce by switchable GC/GC x GC-olfactometry-MS and sensory evaluation [article]. *Food Chemistry, 342*, Article 128224. https://doi.org/10.1016/j.foodchem.2020.128224

Wang, Y. Z., Hu, S. Q., Li, W. J., Gu, J., Yuan, H. R., Ling, X., & Chen, Y. (2019). Chlorine migration mechanisms during torrefaction of fermentation residue from food waste. *Bioresource Technology, 271*, 9–15. https://doi.org/10.1016/j.biortech.2018.08.098

Xu, X., Liu, J. B., Xu, Q., & Wang, R. F. (2025). Recent developments on detection technology for the drying processes of agricultural products. *Technology in Agronomy, 5*(1), Article e013. https://doi.org/10.48130/tia-0025-0008

Xu, X., Liu, J. B., Zhang, T. J., Wang, R. F., Xu, Q., Li, B., & Wei, Z. Z. (2025). Online detection of potato drying stages based on improved YOLOv7-tiny model. *Drying Technology, 43*(4), 679–689. https://doi.org/10.1080/07373937.2025.2450700

Zang, Z. P., Zhang, Q., Huang, X. P., Jiang, C. H., He, C. C., & Wan, F. X. (2023). Effect of ultrasonic combined with vacuum far-infrared on the drying characteristics and physicochemical quality of Angelica sinensis. *Food and Bioprocess Technology, 16*(11), 2455–2470. https://doi.org/10.1007/s11947-023-03076-3

Zhang, W. P., Chen, C., Ju, H. Y., Okaiyeto, S. A., Sutar, P. P., Yang, L. Y., … Xiao, H. W. (2024). Pulsed vacuum drying of fruits, vegetables, and herbs: Principles, applications and future trends. *Comprehensive Reviews in Food Science and Food Safety, 23(5), Article e13430*. https://doi.org/10.1111/1541-4337.13430

Zhao, L. C., Chen, W. B., Zhang, X. F., Li, Y. X., Lv, K. D., & Hu, L. Q. (2024). Advanced fluorescent probes, portable electrochemical and colorimetric sensors for detection of chloride ions in bodily fluids, foods and waters. *Microchemical Journal, 206, Article 111528*. https://doi.org/10.1016/j.microc.2024.111528

Zhou, K., Patrignani, F., Sun, Y.-M., Lanciotti, R., & Xu, Z.-L. (2021). Inhibition of ethyl carbamate accumulation in soy sauce by adding quercetin and ornithine during thermal process [article]. *Food Chemistry, 343, Article 128528*. https://doi.org/10.1016/j.foodchem.2020.128528